Integrated Omics Analysis of the Effects of Nano-Antimicrobial Peptides on the Intestinal Microbiota and Metabolome of Tibetan Sheep

Yaqin Zhao , Xiaoshan Wang , Haixia Jing , Liyuan Zhao , Fengjun Liu *

Posted Date: 12 March 2026

doi: 10.20944/preprints202603.1006.v1

Keywords: Tibetan sheep; nano-antimicrobial peptides; 16S rRNA gene; non-targeted metabolomics

 doi:10.20944/preprints202603.1006.v1

Article

Integrated Omics Analysis of the Effects of Nano-Antimicrobial Peptides on the Intestinal Microbiota and Metabolome of Tibetan Sheep

Yaqin Zhao [1], Xiaoshan Wang [1], Haixia Jing [1], Liyuan Zhao [2] and Fengjun Liu [1,*]

[1] Department of Veterinary Medicine, College of Agriculture and Animal Husbandry, Qinghai University, Xining, 810016, China

[2] Qinghai Vocational and Technical Institute of Animal Husbandry and Vet, Xining, 812100, China

* Correspondence: liufengjuns@126.com

Abstract

This study investigated the effects of dietary nano-antimicrobial peptides (NAPs) on the microbial communities and metabolic profiles in Tibetan sheep. Using 16S rRNA gene high-throughput sequencing and non-targeted metabolomics, the contents of the small intestine, rumen, and rectum were systematically analyzed in a control group (Group A) and a NAP-supplemented group (Group B). Multi-omics integration methods, including O2PLS and Pearson correlation analysis, were employed to explore the association between microbial communities and metabolites. Alpha and beta diversity analyses revealed significant differences ($P < 0.05$) in the microbial community structure of the small intestine between the two groups. In contrast, the rumen and rectal microbiota remained relatively stable, indicating that the regulatory effects of NAPs on the intestinal microecology are site-specific. In the small intestine, NAPs altered the composition of dominant functional microbiota and the abundance of taxa related to energy metabolism. Metabolomic analysis identified significant shifts in metabolic profiles, specifically within the bile acid, fatty acid, and phospholipid pathways ($P < 0.05$). Group A exhibited baseline steady-state characteristics (e.g., cholic acids and phospholipids), whereas Group B showed activation of unsaturated fatty acids and related metabolites. Multi-omics integration revealed a stable systematic association between intestinal microbial genera and metabolites. Specifically, bile acid and prostaglandin metabolites were negatively correlated with *Firmicutes*-related taxa, suggesting a potential role for bile acid metabolism in regulating intestinal microecology and host immunity. These findings suggest that NAP supplementation may contribute to maintaining host energy metabolism and intestinal homeostasis by regulating intestinal microecology.

Keywords: Tibetan sheep; nano-antimicrobial peptides; 16S rRNA gene; non-targeted metabolomics

1. Introduction

Tibetan sheep (*Ovis aries*), a unique and valuable livestock resource on the Qinghai-Tibet Plateau, are primarily distributed in the high-altitude pastoral regions of Qinghai, Tibet, and Gansu provinces, at elevations of around 4,000 meters above sea level. They play a vital role in plateau animal husbandry and the local economy [1]. Over long periods of natural selection, Tibetan sheep have developed a specialized intestinal microecological system that enables them to adapt to harsh environments, including extreme cold, hypoxia, and limited forage availability [2]. The energy acquisition, nutrient conversion, and immune homeostasis of Tibetan sheep heavily rely on a stable and functionally efficient intestinal microbiota.

The intestinal microbiota is a critical regulator of host health, influencing nutrient metabolism, immune function, and disease prevention [3–5]. Previous studies have shown that the microbiota of Tibetan sheep is primarily composed of dominant phyla such as *Firmicutes*, *Bacteroidetes*,

 doi:10.20944/preprints202603.1006.v1

Proteobacteria, and *Actinobacteria* [6,7]. These microorganisms play essential roles in energy metabolism, immune regulation, and the environmental adaptation of plateau ruminants [8–11]. Despite the importance of this microbial community, traditional breeding practices continue to rely heavily on antibiotics to regulate gastrointestinal health. Long-term use of antibiotics, however, can lead to bacterial resistance and food safety concerns, which challenges the sustainable development of animal husbandry [12].

Antimicrobial peptides (AMPs), natural host defense molecules, offer broad-spectrum antibacterial activity without the risk of inducing resistance, making them promising alternatives to antibiotics [13]. Paneth cells, a key source of AMPs, play a crucial role in regulating the intestinal microbiota and maintaining the mucosal barrier by secreting antimicrobial peptides such as α-defensins and lysozyme [5]. Their application has been proven effective in enhancing piglet weight gain, improving dairy cow milk quality, and optimizing ewe lactation performance [13–15]. Recent advancements in nanotechnology have further enhanced the stability and antibacterial efficacy of AMPs, making them even more effective in complex physiological environments and extending their in vivo half-life [16–18]. However, most existing studies focus on poultry and monogastric animals, with limited research on ruminants, particularly Tibetan sheep, and the mechanisms of intestinal microecological responses to nano-antimicrobial peptides (NAPs) remain unclear.

To address this gap, this study aimed to evaluate the effects of dietary NAPs on the intestinal microbiota of Tibetan sheep, using 16S rRNA gene sequencing and non-targeted metabolomics. The goal was to provide a theoretical foundation for green breeding of Tibetan sheep in alpine pastoral areas and the development of novel antibiotic-free feed additives. In this study, the rumen, small intestine, and rectum were selected as sampling sites. The small intestine is the primary site for nutrient digestion and absorption, and its mucosal structure and microbiota directly influence digestive efficiency and host health. As a specialized digestive organ in ruminants, the rumen plays a central role in feed degradation, volatile fatty acid production, and microbial metabolism. The rectum, located at the distal end of the gastrointestinal tract, serve as an indirect indicator of the microecological status of the distal gut. Together, these three sites represent distinct functional regions of the gastrointestinal tract in Tibetan sheep, allowing for a comprehensive understanding of the effects and mechanisms of nano-antimicrobial peptides in the gastrointestinal tract.

2. Materials and Methods

2.1. Ethics Approval

All experimental procedures were approved by the Institutional Animal Care and Use Committee (IACUC) of the College of Veterinary Medicine, Qinghai University (Approval No: SL-2023042; Approval Date: 2023.06.29). Every effort was made to minimize animal suffering and to reduce the number of animals used.

2.2. Animals and Experimental Design

Eighteen non-pregnant Tibetan sheep, weighing 35 ± 3 kg, were obtained from the experimental station of Qinghai University, Qinghai, China. The sheep were randomly assigned to two groups (n = 9 per group): Group A (Control group): fed a basal diet consisting of 500 g concentrate and 300 g hay per sheep/day; Group B (Experimental group): fed the same basal diet as Group A supplemented with 0.125 g of NAPs per sheep/day.

Sheep were housed in standardized individual pens with controlled ventilation, natural lighting, and a regulated environment. All animals had *ad libitum* access to clean drinking water. The facilities were cleaned and disinfected daily to maintain high hygiene standards and minimize environmental stress. Health status was monitored daily by a veterinarian throughout the 30-day experimental period.

 doi:10.20944/preprints202603.1006.v1

2.3. Sample Collection

After 30 days of feeding, all sheep were slaughtered for sample collection. The animals were anesthetized via intravenous injection of sodium pentobarbital (20 mg/kg) and then exsanguinated without prior fasting in order to preserve the natural gastrointestinal contents.

Following laparotomy, the small intestine, rumen, and rectum were isolated. Contents from these three sites were collected and systematically labeled. For Group A, samples were designated as A-a (small intestine), A-b (rumen), and A-c (rectum); Group B samples were similarly labeled as B-a, B-b, and B-c. Each sample (approx. 2 mL) was immediately transferred into sterile 2.5 mL cryovials, snap-frozen in liquid nitrogen, and subsequently transported on dry ice to Gene Denovo Biotechnology Co., Ltd. (Guangzhou, China) for 16S rRNA gene sequencing and metabolomic analysis.

2.4. Bacterial 16S rRNA Gene Sequencing and Analysis

Total genomic DNA was extracted from the gastrointestinal contents using the HiPure Stool DNA Kit (Meiji Biotechnology Co., Ltd., Guangzhou, China) according to the manufacturer's instructions. The concentration and purity of the extracted DNA were assessed using a NanoDrop 2000 spectrophotometer (Thermo Fisher Scientific, USA) to ensure sufficient quality for downstream applications. The V3–V4 hypervariable region of the bacterial 16S rRNA gene was amplified using the universal primers 341F (5′-CCTACGGGNGGCWGCAG-3′) and 806R (5′-GACTACHVGGGTATCTAATCC-3′). PCR amplification was performed using a high-fidelity enzyme system in triplicate to ensure technical consistency. The resulting amplicons were purified using AMPure XP Beads (Beckman Coulter, USA) and quantified with a Qubit 3.0 Fluorometer (Thermo Fisher Scientific, USA). Sequencing libraries were constructed using the Nextera XT Index Kit (Illumina, USA) with unique sample barcodes. After library quality validation, 2 × 300 bp paired-end sequencing was performed on the Illumina MiSeq platform. Raw sequencing data were processed using QIIME 2 (version PE250). Raw paired-end reads were first filtered to remove low-quality sequences and then assembled into tags. These tags underwent further quality control to generate clean tags. Subsequently, sequences were clustered into OTUs, during which chimeric sequences were identified and removed to yield effective tags. Taxonomic classification was assigned to the representative sequence of each OTU using the SILVA database (Release 138) with a confidence threshold of 0.8. Based on the OTU abundance profile, subsequent analyses, including alpha and beta diversity, as well as functional prediction, were performed.

2.5. LC-MS Non-Targeted Metabolomics Detection and Analysis

Samples were thawed and extracted using a pre-cooled mixture of methanol, acetonitrile, and water (2:2:1, v/v). Following vortexing and ultrasonic extraction (30 min, 4 °C), the mixture was kept at −20 °C for 10 min. After centrifugation at 14,000 × g (20 min, 4 °C), the supernatant was collected and evaporated to dryness under vacuum. For final analysis, the residue was redissolved in 100 μL of 50% acetonitrile, vortexed, and centrifuged at 14,000 × g for 15 min at 4 °C to remove any remaining particulates. The final supernatant was collected for injection. Quality Control (QC) samples were prepared by pooling equal aliquots from each test sample to equilibrate the LC-MS system, monitor instrument performance, and ensure experimental reproducibility.

Metabolite separation was performed using an Agilent 1290 Infinity UHPLC system equipped with a HILIC column. The column temperature was maintained at 25 °C, with a flow rate of 0.5 mL/min and an injection volume of 2 μL. Mobile phase A consisted of water containing 25 mM ammonium acetate and 25 mM ammonium hydroxide, while mobile phase B was 100% acetonitrile. The gradient elution program was optimized as follows: 0–0.5 min, 95% B; 0.5–7 min, 95%–65% B; 7–8 min, 65%–40% B; 8–9 min, 40% B; 9–9.1 min, 40%–95% B; and 9.1–12 min, 95% B. Samples were kept in a 4 °C autosampler throughout the analysis, with QC samples inserted into the sequence at regular intervals.

 doi:10.20944/preprints202603.1006.v1

Mass spectrometry was conducted using an AB Triple TOF 6600 system to acquire both primary (MS1) and secondary (MS2) spectra. Electrospray ionization (ESI) source parameters were set as follows: Gas1/Gas2, 60 psi; curtain gas (CUR), 30 psi; ion source temperature, 600 °C; and spray voltage, ±5500 V. The MS1 m/z range was 60–1000 Da with an accumulation time of 0.20 s/spectra. The MS2 m/z range was 25–1000 Da with an accumulation time of 0.05 s/spectra. Data-dependent acquisition (DDA) was performed using the Information-Dependent Acquisition (IDA) mode with a declustering potential of ±60 V and a collision energy of 35 ± 15 eV. Isotope ions were dynamically excluded within 4 Da, and 10 fragment spectra were collected per scan.

To facilitate subsequent analysis, raw spectral data were first converted to the .mzML standard using ProteoWizard. Then the XCMS algorithm was utilized to perform automated peak alignment and retention time adjustment, effectively normalizing the extracted peak areas across all samples..

2.6. Statistical Analysis

For alpha diversity indices, Welch's t-test was used to evaluate differences between groups. Principal Coordinate Analysis (PCoA) based on Bray-Curtis distances was performed to visualize microbial community shifts, with significance assessed via PERMANOVA ($P < 0.05$). To identify specific microbial biomarkers, pairwise intergroup comparisons were conducted using the Wilcoxon rank-sum test. Linear Discriminant Analysis (LDA) Effect Size (LEfSe) was applied to estimate the effect size of each differentially abundant taxon, with an LDA score threshold of > 2.0 and $P < 0.05$. Functional metagenomes were predicted based on the OTU abundance table using PICRUSt2 software to infer Kyoto Encyclopedia of Genes and Genomes (KEGG) pathway enrichment.

Metabolite annotation was performed by matching accurate mass and MS/MS fragments against public databases, including MassBank, METLIN, and MoNA, supplemented by an in-house secondary mass spectrometry database. Differentially abundant metabolites (DAMs) were identified based on the following criteria: Variable Importance in Projection (VIP) ≥ 1 from the OPLS-DA model and $P < 0.05$ from Student's t-test, and $|\log_2 FC| > 1$ (fold change > 2 or < 0.5).

Metabolic pathway enrichment analysis was conducted via the KEGG database, with significance determined by a P value or false discovery rate (FDR) < 0.05 following -log10 transformation. To integrate the two datasets, an O2PLS-DA model was utilized to identify common variation dimensions between the microbiome and metabolome. Spearman correlation analysis was subsequently performed using the pheatmap package in R (version https://CRAN.R-project.org/package=pheatmap) to elucidate associations between differential microbial genera and metabolites.

3. Results

3.1. Analysis of 16S rRNA Gene Sequencing Results

To investigate the effects of NAPs supplementation on the gastrointestinal microbiota of Tibetan sheep, 16S rRNA gene sequencing was performed on gastrointestinal samples collected from Groups A and B after 30 days of feeding. After quality control and filtering, more than 80% of raw reads were retained as high-quality sequences for each sample. The number of effective tags exceeded 40,000 per sample, indicating sufficient sequencing depth for reliable downstream analyses. Statistical evaluation of Operational Taxonomic Unit counts (OTUs) and sequencing depth metrics was conducted (Figure 1). Variations in OTUs and tag counts were observed among samples, reflecting differences in microbial richness across groups. These results established the basis for subsequent analyses of microbial community structure and diversity.

 doi:10.20944/preprints202603.1006.v1

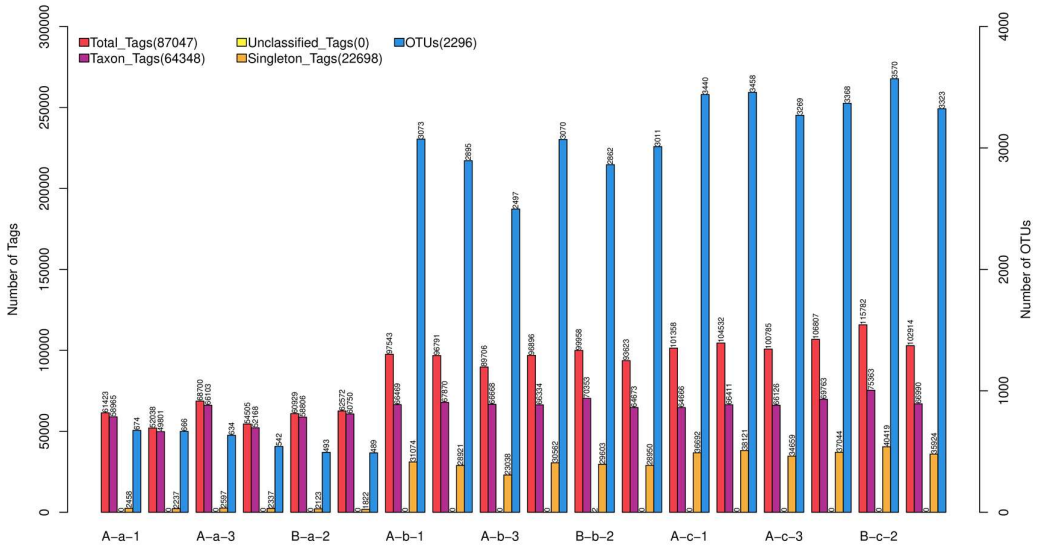

Figure 1. Distribution of sequencing tag counts and OTUs across all samples.

3.2. *Alpha Diversity Analysis*

The OTUs in each sample were ranked according to their relative abundance to construct rank–abundance curves. Along the horizontal axis, the length of the curve reflects species richness, with a longer curve indicating a greater number of OTUs. Along the vertical axis, the slope of the curve represents species evenness; a flatter curve indicates a more even distribution of species abundance within the sample. As shown in Figure 2, samples A-a and B-a demonstrated relatively steeper slopes compared with other groups, indicating reduced species evenness. In contrast, the remaining groups exhibited flatter curves, suggesting a more homogeneous distribution of microbial taxa.

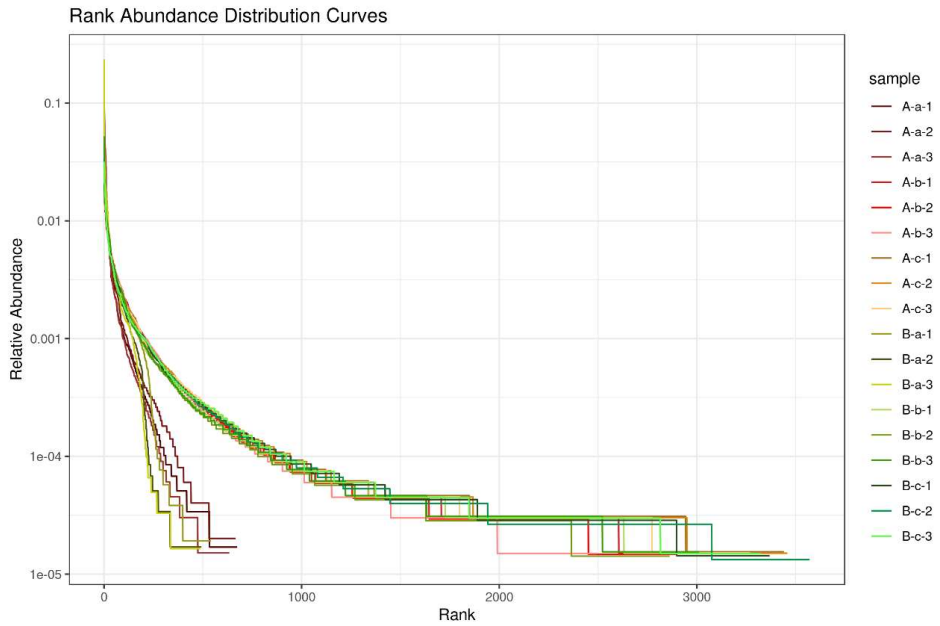

Figure 2. Rank–abundance curves of microbial communities in different samples.

Based on Welch's t-test, alpha diversity analysis using the Sob, Chao1, and ACE indices (Table 1) revealed significant differences ($P < 0.05$) in community richness between groups A-a and B-a.

 doi:10.20944/preprints202603.1006.v1

However, no significant differences in species richness were observed between groups A-b and B-b or between groups A-c and B-c.

Table 1. Alpha diversity comparison based on Sob, Chao1, and ACE indices.

Group	Sob (*P* value)	Chao1 (*P* value)	ACE (*P* value)
A-a vs B-a	0.0029	0.0191	0.0062
A-b vs B-b	0.4549	0.4242	0.4097
A-c- vs B-c	0.7635	0.7670	0.8353

3.3. Beta Diversity Analysis

PCoA was performed to evaluate differences in microbial community structure among groups. In the PCoA plot, samples positioned closer together indicate more similar microbial community compositions, whereas greater separation reflects increased compositional dissimilarity. As shown in Figure 3 and Table 2, a significant difference in microbial community structure was observed between groups A-a and B-a ($P < 0.05$). In contrast, no significant differences were detected between groups A-b and B-b or between groups A-c and B-c ($P > 0.05$). These results were consistent with the alpha diversity analysis.

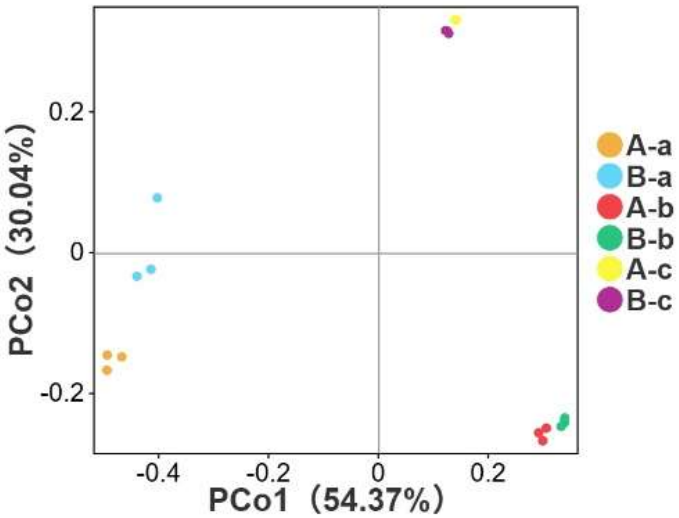

Figure 3. Principal coordinate analysis (PCoA) of microbial community structure among different groups.

Table 2. PERMANOVA analysis of beta diversity among groups.

Group	*P* value
A-a vs B-a	0.03
A-b vs B-b	0.14
A-c vs B-c	0.07

3.4. Differential Microbial Composition Analysis

Based on the results of the alpha and beta diversity analyses, significant differences in microbial richness and community structure were observed between groups A-a and B-a, whereas no significant differences were detected between groups A-b and B-b or between groups A-c and B-c. Therefore, subsequent microbial composition analysis focused on groups A-a and B-a. The results are

 doi:10.20944/preprints202603.1006.v1

presented in Table 3. The top 10 dominant genera in both groups showed a largely similar taxonomic composition, with *Candidatus_Saccharimonas*, *Christensenellaceae_R7_group*, *Ruminococcus*, *NK4A214_group*, and *Saccharofermentans* constituting the core microbiota. However, notable differences were observed in their relative abundances. In group A-a, *Candidatus_Saccharimonas* was the most abundant genus, whereas in group B-a, *Saccharofermentans* became the predominant genus, and *Candidatus_Saccharimonas* decreased to second place. These findings suggest that NAPs supplementation did not alter the core taxonomic composition of the intestinal microbiota in Tibetan sheep but significantly reshaped the relative abundance structure of dominant genera.

Table 3. Relative abundances (%) of the top 10 dominant genera in groups A-a and B-a (mean ± SD).

Genus	A-a-1/B-a-1	A-a-2/B-a-2	A-a-3/B-a-3	Mean±SD
Group A				
Candidatus_Saccharimonas	35.3091	28.1601	36.7487	33.4060 ± 4.5997
Christensenellaceae_R-7_group	3.0001	3.7911	3.0468	3.2793 ± 0.4438
Ruminococcus	2.7321	2.8092	1.8880	2.4764±0.5111
NK4A214_group	1.5246	1.5743	2.1102	1.7364±0.3247
Saccharofermentans	1.3109	1.0843	1.6868	1.3607 ± 0.3043
Xylanibacter	0.2273	0.9036	0.2723	0.4677 ± 0.3781
UCG-005	0.0594	0.0161	0.0545	0.0433 ± 0.0237
Rikenellaceae_RC9_gut_group	0.0356	0.4377	0.0257	0.1663 ± 0.2351
Treponema	0.0153	0.0281	0.0076	0.0170 ± 0.0104
Bacteroides	0.0034	0.0080	0.0045	0.0053 ± 0.0024
Group B				
Saccharofermentans	12.7933	20.9417	23.6148	19.1166 ± 5.6369
Candidatus_Saccharimonas	16.1843	11.4155	9.0831	12.2276 ± 3.6196
Christensenellaceae_R-7_group	3.1475	4.6747	5.0815	4.3012 ± 1.0197
NK4A214_group	3.0114	2.2583	2.5926	2.6208 ± 0.3774
Xylanibacter	3.0133	0.5459	0.2699	1.2764 ± 1.5105
Ruminococcus	1.6600	0.94038	1.0140	1.2048 ± 0.3959
Treponema	0.9929	0.0002	0.0082	0.3338 ± 0.5708
Rikenellaceae_RC9_gut_group	0.7150	0.0238	0.0280	0.2556 ± 0.3979
UCG-005	0.1591	0.0357	0.0807	0.0918 ± 0.0624
Bacteroides	0.0077	0.0017	0.0066	0.0053 ± 0.003

Based on the significant differences observed in alpha and beta diversity between groups A-a and B-a, linear discriminant analysis effect size (LEfSe) was performed to identify taxa that were differentially enriched between the two groups. The results are shown in Figure 4. The LEfSe analysis revealed that *Bacillota*, *Bacteria*, *Bacteroidota*, and *Pseudomonadota* were significantly enriched in group B-a. In contrast, *Patescibacteria*, *Archaea*, *Methanobacteriota*, *Myxococcota*, and *Nitrospirota* were significantly enriched in group A-a.

 doi:10.20944/preprints202603.1006.v1

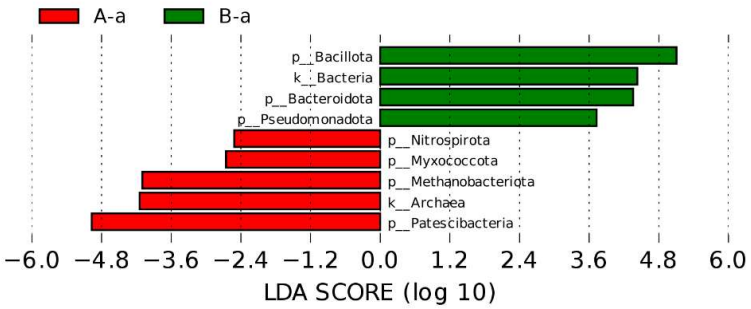

Figure 4. LEfSe analysis identifying differentially enriched taxa between groups A-a and B-a.

3.5. Functional Prediction of Microbial Communities

Based on the significant differences observed in alpha diversity, beta diversity, and LEfSe analyses, functional prediction of the microbial communities was conducted. The results are shown in Figure 5. At KEGG, metabolism was the predominant functional category in both groups A-a (Figure 5A) and B-a (Figure 5B). Within this category, carbohydrate metabolism showed the highest relative abundance, followed by metabolism of cofactors and vitamins and amino acid metabolism. Genetic information processing represented the second most abundant functional module in both groups. Although the overall functional profiles were similar between A-a and B-a, differences were observed in the relative abundances of several metabolic pathways, suggesting that NAPs supplementation may have modulated functional potential without fundamentally altering core metabolic functions.

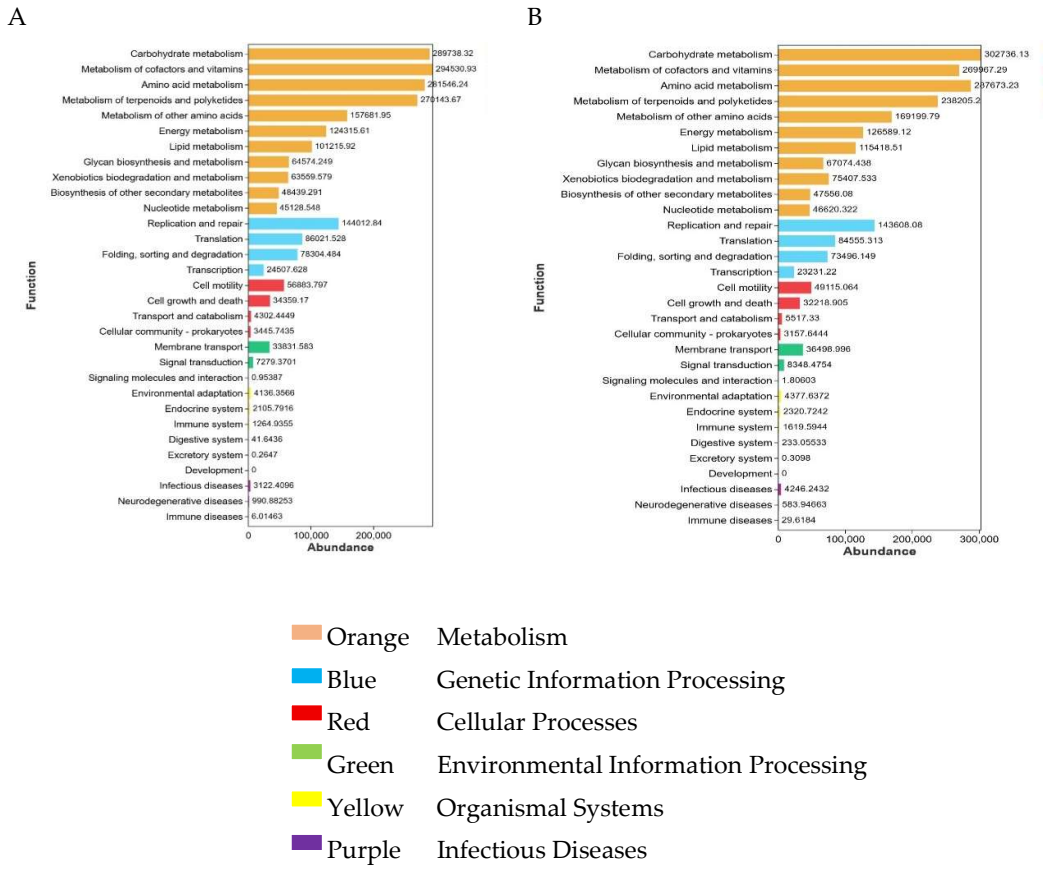

Figure 5. Functional prediction of microbial communities based on KEGG pathways in groups A-a and B-a. A, A-a; B, B-a.

 doi:10.20944/preprints202603.1006.v1

The above results indicate that although the overall taxonomic composition of the core microbiota remained stable between groups A-a and B-a, the relative abundances of dominant taxa were altered. This suggests that NAPspeptide supplementation may influence gastrointestinal metabolic potential by modulating the proportional distribution of key microbial taxa. Functional prediction analysis further demonstrated that no significant differences were observed in the overall functional gene profiles between the two groups. However, variations in the relative abundances of specific metabolic pathways were detected, implying potential shifts in microbial functional capacity. To further elucidate the impact of NAPs on gastrointestinal metabolism in Tibetan sheep, non-targeted metabolomic analysis was subsequently performed. The results are presented below.

3.6. Analysis of Non-Targeted Metabolomics Results

To evaluate data quality and analytical stability, the combined positive and negative ion datasets were subjected to principal component analysis (PCA), including QC samples (Figure 6). The PCA score plot showed that QC samples were tightly clustered, with overlapping distribution in the multivariate space, indicating good analytical reproducibility and system stability throughout the experiment. Metabolite identification and annotation were subsequently performed (Table 4). A total of 18,102 metabolite features were detected, including 9,793 in positive ion mode and 8,309 in negative ion mode. Among these, 3,916 positive ion features and 3,521 negative ion features were successfully annotated to known metabolites.

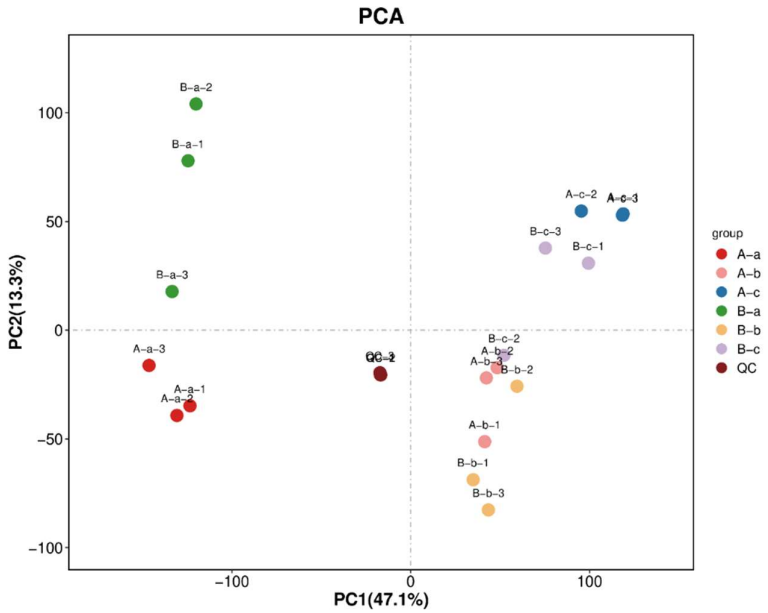

Figure 6. PCA score plot of combined positive and negative ion datasets including QC samples.

Table 4. Summary of metabolite detection and annotation results in positive and negative ion modes.

Type	All	known	Unknown
POS	9793	3916	5877
NEG	8309	3521	4788

3.7. Differential Metabolite Profiling Between Groups

Based on the abundance matrix containing 7,437 annotated metabolite features retained across all samples, differential metabolite analysis was performed between Group A (control) and Group B (experimental). Metabolites were screened using the criteria of $\log_2$ fold change (FC＞1) or (FC＜-

 doi:10.20944/preprints202603.1006.v1

1)and $P < 0.05$. The distribution of differential metabolites is presented as volcano plots in Figure 7. In the plots, red dots represent upregulated metabolites, whereas yellow dots indicate downregulated metabolites. Overall, more metabolites were downregulated than upregulated in all comparisons.. Notably, several downregulated metabolites exhibited high variable importance in projection (VIP) values, suggesting that these metabolites contributed substantially to group discrimination and may represent key metabolites distinguishing Group A from Group B.

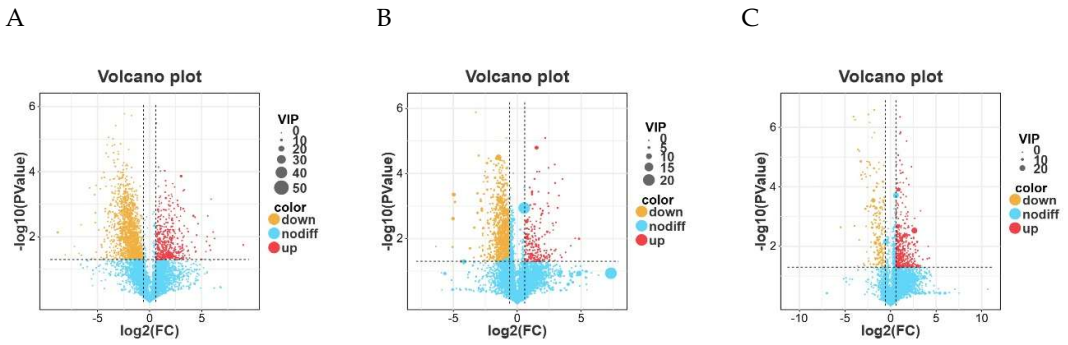

Figure 7. Volcano plots showing differential metabolites between A-a and B-a (A), A-b and B-b (B), and A-c and B-c (C).

A statistical summary of differentially expressed metabolites between groups is presented in Figure 8. In the comparison between A-a and B-a, 444 metabolites were upregulated and 1,424 were downregulated in group B-a relative to group A-a. Similarly, in the A-b vs. B-b comparison, 199 metabolites were upregulated and 1,114 were downregulated. In contrast, the A-c vs. B-c comparison showed 432 upregulated and 203 downregulated metabolites. Overall, the number of downregulated metabolites exceeded that of upregulated metabolites in the A-a vs. B-a and A-b vs. B-b comparisons, whereas the opposite trend was observed in the A-c vs. B-c comparison.

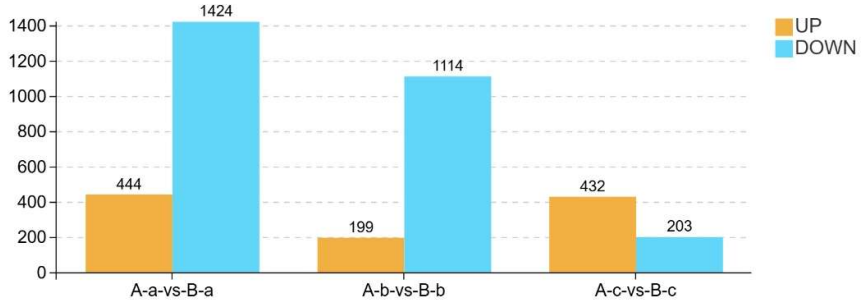

Figure 8. Summary of differentially expressed metabolites in combined ion mode.

Differential metabolite analysis further identified key discriminative metabolites between groups A and B based on variable importance in projection (VIP) scores derived from the OPLS-DA model (Figure 9). In the A-a vs. B-a comparison, glycocholic acid, linoleic acid, glycerophosphocholine, oleic acid, and lysophosphatidylcholine (18:2) were enriched in group B-a, whereas cholic acid, 1-stearoyl-2-hydroxy-sn-glycero-3-phosphocholine, 1-palmitoyl-sn-glycero-3-phosphocholine, deoxycholic acid, D-desthiobiotin, trihydroxycholan-24-oic acid, and 15-cyclohexylpentanorprostaglandin F2α were enriched in group A-a. In the A-b vs. B-b comparison, hexadecanedioic acid, leptomycin B, and (−)-O-acetyl-D-mandelic acid were enriched in group B-b, whereas 15-cyclohexylpentanorprostaglandin F2α, pentadecanoic acid, enterolactone, heptadecanoic acid, 3α,7α-dihydroxy-12-oxocholanoic acid, and cholesterol sulfate were enriched in group A-b. Similarly, in the A-c vs. B-c comparison, (2E,4E)-12-hydroxy-13-(hydroxymethyl)-14-methoxy-3,5,7-

 doi:10.20944/preprints202603.1006.v1

trimethyl-14-oxotetradeca-2,4-dienoic acid, 15-ketoprostaglandin F2α, palmitoleoyl ethanolamide, leptomycin B, and aurantio-obtusin were enriched in group B-c, whereas 1H-pyrazole-3-carboxylic acid, pheophorbide a, antimycin A, and 1-palmitoyl-2-oleoyl-phosphatidylglycerol were enriched in group A-c.

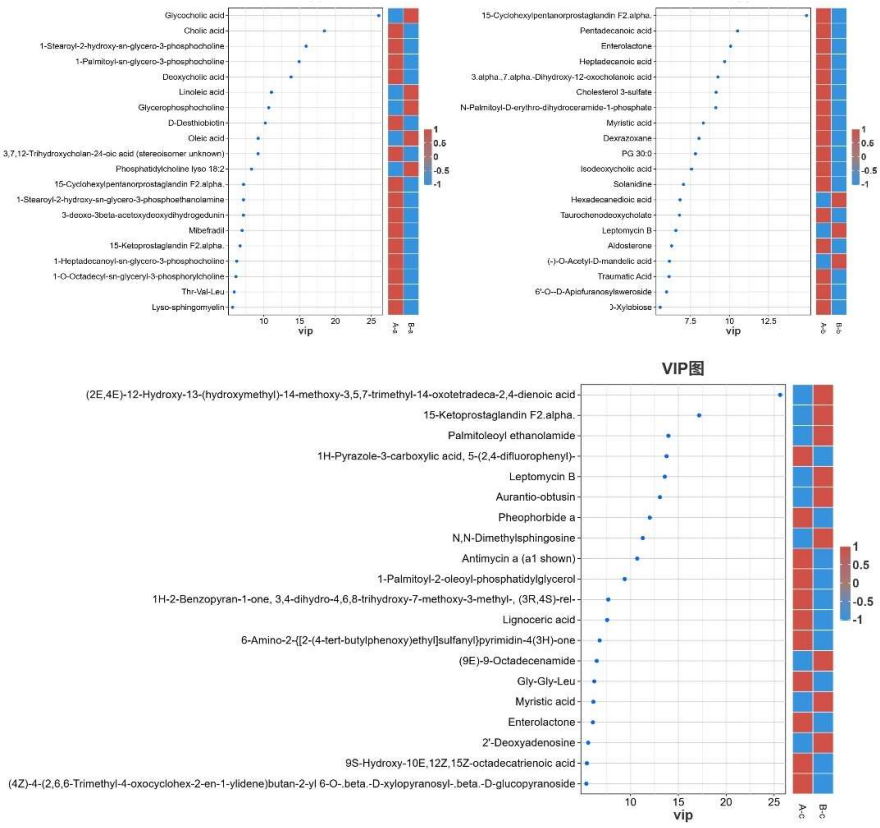

Figure 9. VIP plots of differential metabolites for A-a vs B-a (A), A-b vs B-b (B), and A-c vs B-c (C).

3.8. KEGG Pathway Enrichment Analysis of Differential Metabolites Between Groups

Differential metabolites were mapped to the KEGG database for pathway enrichment analysis. A hypergeometric test was applied to identify pathways significantly enriched in differential metabolites relative to the overall metabolite background. As shown in Figure 10A, several pathways were significantly enriched in the A-a vs. B-a comparison, including choline metabolism in cancer, histidine metabolism, and primary bile acid biosynthesis. In contrast, no significantly enriched pathways were detected in the A-b vs. B-b comparison (Figure 10B). Only a limited number of pathways were enriched in the A-c vs. B-c comparison (Figure 10C), including alpha-linolenic acid metabolism and biosynthesis of unsaturated fatty acids.

 doi:10.20944/preprints202603.1006.v1

A

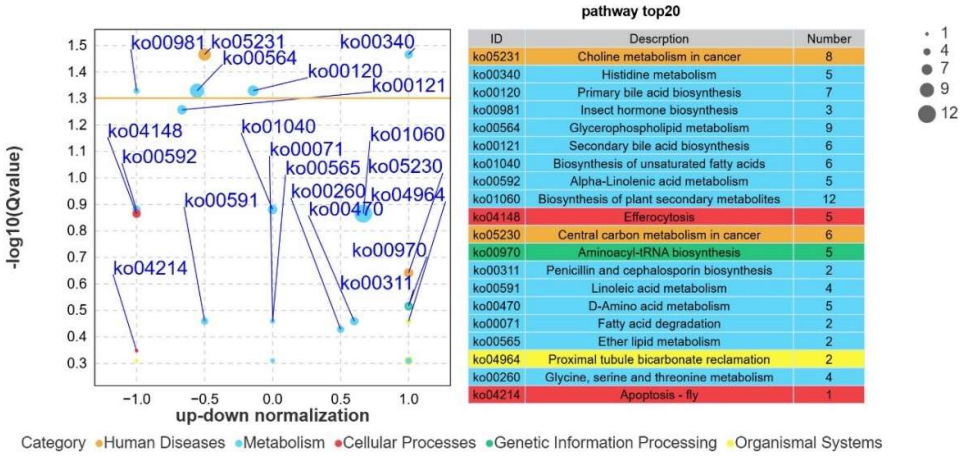

ID	Descrption	Number
ko05231	Choline metabolism in cancer	8
ko00340	Histidine metabolism	5
ko00120	Primary bile acid biosynthesis	7
ko00981	Insect hormone biosynthesis	3
ko00564	Glycerophospholipid metabolism	9
ko00121	Secondary bile acid biosynthesis	6
ko01040	Biosynthesis of unsaturated fatty acids	6
ko00592	Alpha-Linolenic acid metabolism	5
ko01060	Biosynthesis of plant secondary metabolites	12
ko04148	Efferocytosis	5
ko05230	Central carbon metabolism in cancer	6
ko00970	Aminoacyl-tRNA biosynthesis	5
ko00311	Penicillin and cephalosporin biosynthesis	2
ko00591	Linoleic acid metabolism	4
ko00470	D-Amino acid metabolism	5
ko00071	Fatty acid degradation	2
ko00565	Ether lipid metabolism	2
ko04964	Proximal tubule bicarbonate reclamation	2
ko00260	Glycine, serine and threonine metabolism	4
ko04214	Apoptosis - fly	1

B

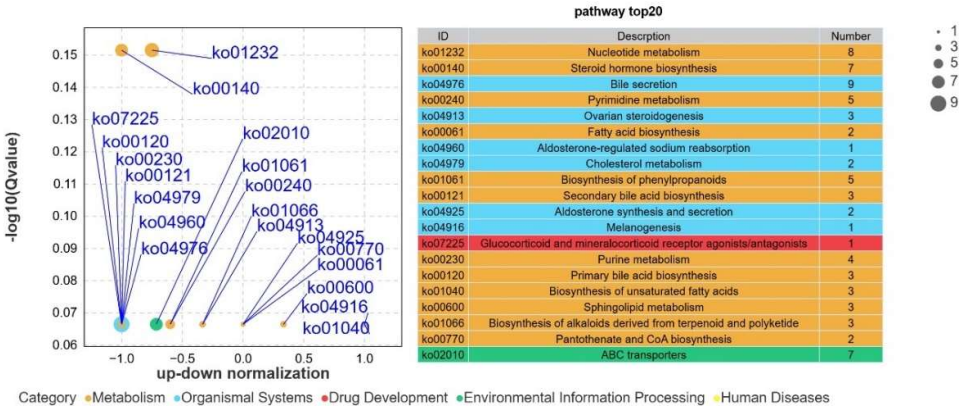

ID	Descrption	Number
ko01232	Nucleotide metabolism	8
ko00140	Steroid hormone biosynthesis	7
ko04976	Bile secretion	9
ko00240	Pyrimidine metabolism	5
ko04913	Ovarian steroidogenesis	3
ko00061	Fatty acid biosynthesis	2
ko04960	Aldosterone-regulated sodium reabsorption	1
ko04979	Cholesterol metabolism	2
ko01061	Biosynthesis of phenylpropanoids	5
ko00121	Secondary bile acid biosynthesis	3
ko04925	Aldosterone synthesis and secretion	2
ko04916	Melanogenesis	1
ko07225	Glucocorticoid and mineralocorticoid receptor agonists/antagonists	1
ko00230	Purine metabolism	4
ko00120	Primary bile acid biosynthesis	3
ko01040	Biosynthesis of unsaturated fatty acids	3
ko00600	Sphingolipid metabolism	3
ko01066	Biosynthesis of alkaloids derived from terpenoid and polyketide	3
ko00770	Pantothenate and CoA biosynthesis	2
ko02010	ABC transporters	7

C

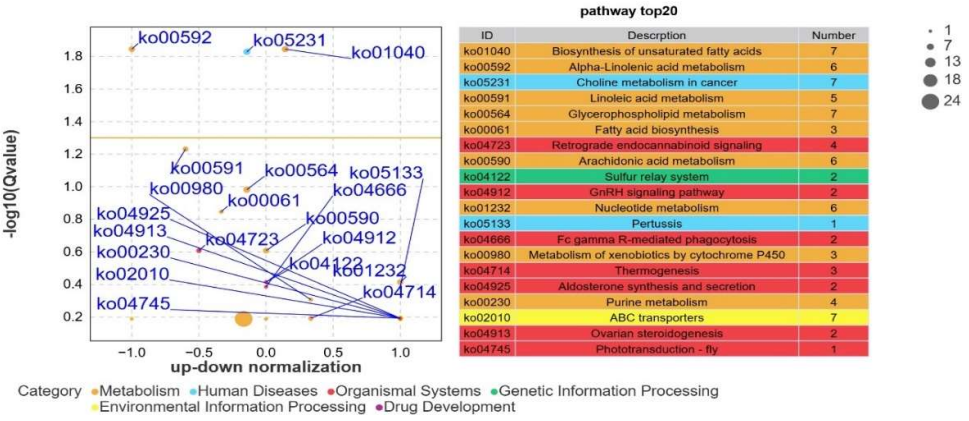

ID	Descrption	Number
ko01040	Biosynthesis of unsaturated fatty acids	7
ko00592	Alpha-Linolenic acid metabolism	6
ko05231	Choline metabolism in cancer	7
ko00591	Linoleic acid metabolism	5
ko00564	Glycerophospholipid metabolism	7
ko00061	Fatty acid biosynthesis	3
ko04723	Retrograde endocannabinoid signaling	4
ko00590	Arachidonic acid metabolism	6
ko04122	Sulfur relay system	2
ko04912	GnRH signaling pathway	2
ko01232	Nucleotide metabolism	6
ko05133	Pertussis	1
ko04666	Fc gamma R-mediated phagocytosis	2
ko00980	Metabolism of xenobiotics by cytochrome P450	3
ko04714	Thermogenesis	3
ko04925	Aldosterone synthesis and secretion	2
ko00230	Purine metabolism	4
ko02010	ABC transporters	7
ko04913	Ovarian steroidogenesis	2
ko04745	Phototransduction - fly	1

Figure 10. KEGG pathway enrichment analysis of differential metabolites. Note: The yellow line indicates the significance threshold corresponding to $P = 0.05$ (−log10 P value). Pathways above this threshold are considered significantly enriched.

Non-targeted metabolomics analysis indicated that, unlike the significant pathway enrichment observed in the A-a vs. B-a comparison, no significantly enriched pathways were detected between A-b and B-b. This suggests that the differential metabolites identified in these two subgroups did not converge into coordinated pathway-level alterations but were more likely to represent isolated

 doi:10.20944/preprints202603.1006.v1

metabolic fluctuations with limited systemic impact. In contrast, a small number of pathways were enriched in the A-c vs. B-c comparison, including alpha-linolenic acid metabolism and biosynthesis of unsaturated fatty acids. Combined with the profile of differential metabolites in this subgroup, these findings suggest potential localized modulation of lipid metabolism. However, no extensive pathway activation or inhibition was observed. Overall, these results indicate that the most pronounced and coordinated metabolic alterations occurred in the A-a vs. B-a comparison, highlighting this subgroup as the primary focus of metabolic regulation in the present study.

3.9. Integrated Analysis of 16S rRNA Gene Sequencing and Non-Targeted Metabolomics

To further investigate the overall associations between the intestinal microbiota (genus level) and the metabolomic profiles of Tibetan sheep following NAPs supplementation, an integrative multi-omics analysis was conducted. An orthogonal two-way partial least squares (O2PLS) model was constructed to evaluate the covariance structure between the microbiome and metabolome datasets. The contribution statistics of the O2PLS model are summarized in Table 5.

Table 5. O2PLS model performance and contribution statistics for integrated microbiome–metabolome analysis.

Model	R2X	R2Y	R2Xcorr	R2Ycorr
Genus	0.838	0.873	0.664	0.838

The shared variation between the microbiome and metabolome datasets was extracted using the O2PLS model. As shown in Figure 11A, genera such as *Syntrophococcus* and *Family_XIII_UCG-001* were distributed on the left side of the loading plot, whereas *Intestinimonas* and *Oscillospira* were located on the right side, indicating distinct contributions of different genera to the integrative model. Similarly, in Figure 11B, metabolites such as prenosterone and ethylmorphine were positioned in the upper right quadrant, while talkoxydir and sulfate were located in the lower right quadrant, suggesting functional differentiation among metabolites within the integrated association structure. To further clarify the association patterns between the intestinal microbiota (genus level) and metabolomic profiles, a Spearman correlation heatmap was constructed using the R package pheatmap based on genus-level microbial abundance and differential metabolites. The results are shown in Figure 12. Metabolites and genera clustered within the same color blocks exhibited similar correlation patterns, implying potential involvement in related metabolic pathways or physiological processes. Terbutaline and 2-dhahba (dmed-fahfa) showed significant positive correlations ($P < 0.05$) with certain genera, including *Lacrimispora*. In contrast, most metabolites, such as prostaglandin D3 and chenodeoxycholic acid, displayed significant negative correlations ($P < 0.05$) with genera including *Lacrimispora* and *Clostridium_methylpentosum*.

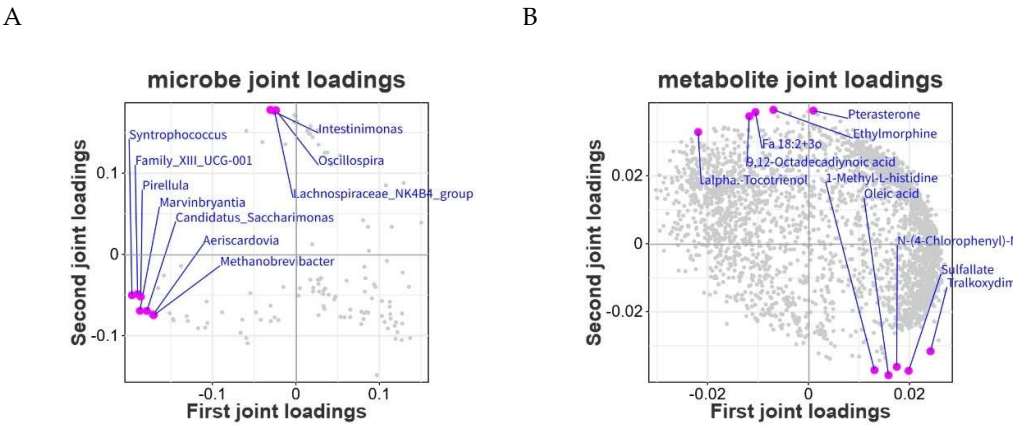

Figure 11. O2PLS loading plot for integrated analysis of genus-level microbiota and metabolomic profiles.

 doi:10.20944/preprints202603.1006.v1

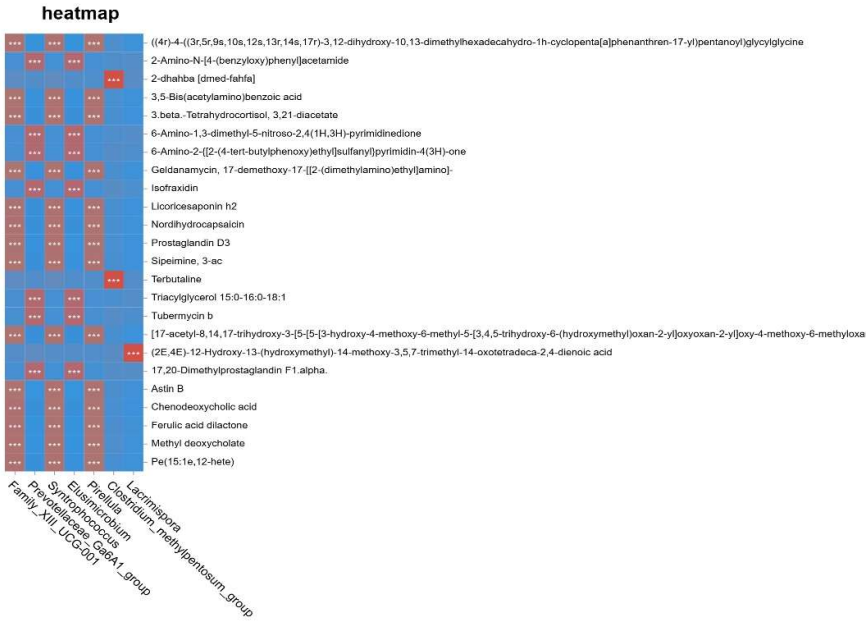

Figure 12. Correlation heatmap of integrated microbiome–metabolome analysis at the genus level. Note: The horizontal axis represents genera, and the vertical axis represents differential metabolites. Each cell indicates the Spearman correlation coefficient between microbial abundance and metabolite levels. Red denotes significant positive correlations, and blue denotes significant negative correlations ($P < 0.05$).

The correlation network exhibited a clear modular structure, in which distinct microbial genera and metabolites formed relatively independent interaction clusters, reflecting the complexity and specificity of microbiome–metabolome associations in the intestinal ecosystem of Tibetan sheep. Within the network, genera such as *Lachnospiraceae_NK4A136_group*, *Dialister*, and *Aerotrigona* functioned as highly connected nodes, suggesting their potential roles as key hubs in host metabolic regulation. *Lachnospiraceae_NK4A136_group* is known to participate in short-chain fatty acid (SCFA) production, and its positive correlations with specific metabolites may indicate its involvement in dietary fiber fermentation and subsequent metabolic processes. *Dialister*, an acid-producing genus, showed associations with metabolites potentially related to intestinal acidification and barrier function. Similarly, the positive correlations observed between *Aerotrigona* and several metabolites may reflect its potential contribution to carbohydrate metabolism or host energy regulation.

 doi:10.20944/preprints202603.1006.v1

Figure 13. Integrated microbiome–metabolome correlation network at the genus level. Note: Blue nodes represent metabolites, and orange nodes represent microbial genera. Red edges indicate significant positive correlations, whereas blue edges indicate significant negative correlations. Edge thickness reflects the strength of the correlation coefficient, and node size corresponds to the degree of connectivity (number of associations).

4. Discussion

Based on 16S rRNA gene sequencing and non-targeted metabolomics, this study systematically evaluated the effects of NAPs supplementation on the microbial community structure and metabolic profiles of different gastrointestinal sites in Tibetan sheep and further explored the potential associations between the microbiome and metabolome. Quality control results demonstrated adequate sequencing depth and a high proportion of high-quality reads that met the technical specifications for gastrointestinal microbial research in ruminants [19], indicating robust and reliable data for downstream analyses. Rank–abundance and alpha diversity analyses revealed significant differences in microbial richness and evenness in the small intestinal contents between the experimental and control groups. Consistently, beta diversity analysis showed clear separation of small intestinal microbial communities between groups, whereas no significant differences were observed at other gastrointestinal sites. These findings suggest that NAPs supplementation exerts site-specific modulation of the intestinal microbiota in Tibetan sheep, with the small intestine appearing particularly responsive. Although the dominant core genera were largely conserved between groups, shifts in their relative abundances were observed. Functional prediction analysis further indicated that while the overall functional gene profiles were not significantly altered, variations in the relative abundance of specific metabolic pathways were detected. Together, these results imply that NAPs may influence gastrointestinal microbial function primarily through modulation of taxonomic structure rather than through large-scale restructuring of the core microbial community.

Metabolomic analysis further demonstrated distinct metabolic profiles between the experimental and control groups. The tight clustering of QC samples confirmed the stability and reproducibility of the analytical platform [20]. A total of 18,102 metabolite features were detected, and differential analysis was performed based on 7,437 annotated compounds consistently retained across all samples. Using $|\log_2 FC| \geq 1.5$ and $P < 0.05$ as screening criteria, differential metabolites were primarily enriched in pathways related to bile acid metabolism, fatty acid metabolism, and phospholipid metabolism. In Group A, higher levels of cholic acid, deoxycholic acid, and

 doi:10.20944/preprints202603.1006.v1

trihydroxycholan-24-oic acid were observed. These bile acids are central components of the bile acid metabolic pathway and play essential roles in cholesterol conversion, lipid digestion, and nutrient absorption. Previous studies have also highlighted the close relationship between bile acid homeostasis, intestinal microecology, and lipid metabolism [21]. Additionally, elevated levels of phosphatidylcholine-related metabolites, including 1-stearoyl-2-hydroxy-sn-glycero-3-phosphocholine and 1-palmitoyl-sn-glycero-3-phosphocholine, may reflect maintenance of membrane structural integrity and lipid transport capacity [22]. The higher abundance of D-desthiobiotin and related biotin derivatives further suggests active participation in fundamental metabolic processes such as fatty acid synthesis and amino acid metabolism. Collectively, these findings indicate that the metabolic profile of Group A was characterized by relatively stable bile acid and phospholipid metabolism. In contrast, Group B exhibited increased levels of unsaturated fatty acids, including linoleic acid and oleic acid. These metabolites are closely associated with lipid metabolic balance, membrane fluidity, and inflammatory regulation [23]. Such changes may reflect adaptive adjustments in lipid metabolism following NAPs supplementation. Moreover, the elevated abundance of glycocholic acid and phospholipid-related intermediates, such as lysophosphatidylcholine (18:2) and glycerophosphocholine, suggests modulation of phospholipid turnover and remodeling processes, potentially influencing membrane dynamics and lipid-mediated signaling [24]. Taken together, the coordinated alterations in bile acid and phospholipid metabolism in Group B imply a restructuring of lipid metabolic networks rather than a complete disruption of metabolic homeostasis.

The differential metabolites were analyzed for pathway enrichment using a hypergeometric test. The results revealed significant enrichment in several pathways in the A-a vs. B-a comparison, such as choline metabolism in cancer, histidine metabolism, and primary bile acid biosynthesis. In contrast, no notable pathway enrichment was found in the A-b vs. B-b comparison, and only a few pathways, including alpha-linolenic acid metabolism and unsaturated fatty acid biosynthesis, were enriched in the A-c vs. B-c comparison. Interestingly, a clear functional relationship between the metabolites and enriched pathways was observed in the A-a vs. B-a comparison.. Group A-a exhibited higher levels of primary bile acids and phosphatidylcholine-related metabolites, which may reflect relatively stable bile acid biosynthesis and membrane-associated lipid metabolism. In contrast, Group B-a showed elevated levels of conjugated bile acids, phospholipid metabolism intermediates, and unsaturated fatty acids, suggesting a potential shift in metabolic flux within these pathways. These findings suggest that bile acid and lipid metabolic pathways may be the central nodes in the metabolic response to NAPs supplementation. Future studies integrating targeted metabolite quantification and functional validation experiments will be necessary to determine whether these metabolic alterations directly mediate the physiological effects observed.

From the perspective of microbiome–metabolome integration, the dynamic coupling between intestinal microbial communities and host metabolic networks is widely considered a key mechanism underlying physiological homeostasis [25]. To characterize the co-variation structure between these two omics layers, an O2PLS model combined with Spearman correlation analysis and heatmap visualization was applied to explore potential associations between microbial genera and metabolites. The results indicated that terbutaline and 2-dhahba (dmed-fahfa) were significantly positively correlated with the genus *Lacrimispora*. This association suggests that *Lacrimispora* may be linked to fatty acid– or steroid-related metabolic processes. As a member of the phylum *Firmicutes*, *Lacrimispora* is commonly regarded as an intestinal fermentative bacterium and has been reported to participate in fatty acid metabolism and related pathways [26]. Therefore, fluctuations in its abundance may be associated with changes in lipid-related metabolic activity. In contrast, several metabolites, including prostaglandin D3 and chenodeoxycholic acid, showed significant negative correlations with genera such as *Lacrimispora* and *Clostridium_methylpentosum*. Chenodeoxycholic acid, an important bile acid component, plays essential roles in lipid digestion, absorption, and microbial ecological regulation [27]. Previous studies have also reported inhibitory effects of certain bile acids on *Firmicutes* taxa [28]. Accordingly, the observed negative correlations are consistent with

 doi:10.20944/preprints202603.1006.v1

the regulatory role of bile acids in modulating gut microbial composition. These findings suggest a potential bidirectional interaction in which bile acid metabolites and specific microbial taxa may jointly contribute to the maintenance of intestinal ecological balance.

Overall, this study revealed a multi-level ecological response of the Tibetan sheep intestine to NAPs supplementation. The small intestine exhibited greater sensitivity to exogenous intervention, as reflected by the clear separation of microbial community structure and dynamic modulation of associated metabolic pathways. At the metabolic level, differential enrichment of bile acid, fatty acid, and phospholipid metabolic pathways suggests that NAPs supplementation may influence host energy balance and membrane-associated functions through coordinated regulation of lipid metabolism and bile acid homeostasis [29].Integrated microbiome–metabolome analysis further demonstrated that within the shared variation dimension of bile acid metabolism and lipid-related metabolites [30], specific genera (e.g., *Lacrimispora*) were significantly associated with multiple metabolites. These associations imply the existence of a potential regulatory network in which microbial metabolism and host-derived metabolic products interact bidirectionally to maintain intestinal ecological balance [31].

It should be noted that these conclusions are derived from statistical associations and inferred biological relevance, therefore carry inherent uncertainty. Functional prediction based on 16S rRNA gene sequencing is constrained by annotation limitations and indirect inference. Although differential metabolite identification and pathway enrichment analyses provide valuable mechanistic clues, causal relationships remain to be validated through targeted metabolite quantification, functional assays, and integration with metagenomic or transcriptomic approaches [32]. Future studies should focus on: (i) high-resolution functional annotation and metabolic pathway reconstruction based on metagenomic or transcriptomic sequencing; (ii) time-series experimental designs to evaluate the dynamic effects and regulatory boundaries of NAPs supplementation; and (iii) mechanistic validation of key microbe–metabolite interactions identified in this study. In summary, this work provides multi-level evidence for understanding the interplay between intestinal microecology and host metabolism in Tibetan sheep and highlights the potential modulatory effects of NAPs supplementation on microbial community structure and metabolic networks across different gastrointestinal sites.

5. Conclusions

This study demonstrates that the small intestine is the primary site of microecological response to NAP supplementation in Tibetan sheep. While the core microbiota remained relatively stable, NAPs significantly reshaped the microbial community structure and diversity ($P < 0.05$). Integrated omics analysis revealed that these microbial shifts were intrinsically linked to systematic alterations in bile acid, fatty acid, and phospholipid metabolic pathways. Specifically, the strong correlations between key genera and metabolites, such as bile acids and prostaglandins, suggest that NAPs maintain intestinal homeostasis by regulating intestinal microecology and host metabolism. These findings provide a theoretical basis for the application of NAPs as precise, site-specific feed additives to enhance gastrointestinal health and metabolic efficiency in ruminants.

Author Contributions: Yaqin Zhao: Conceptualization, Methodology, Formal analysis, Data curation, Writing—original draft. Xiaoshan Wang: Investigation, Resources, Animal husbandry. Haixia Jing: Supervision, Validation, Project administration. Liyuan Zhao: Sample collection. Fengjun Liu: Conceptualization, Funding acquisition, Supervision, Writing—review & editing, Final approval. All authors have read and agreed to the published version of the manuscript.

Funding: This work was supported by the Natural Science Foundation of Qinghai Province (Grant No. 2025-NK-P58). The funding body played no role in the study design, data collection, statistical analysis, manuscript preparation, or the decision to submit the work for publication.

 doi:10.20944/preprints202603.1006.v1

Institutional Review Board Statement: All experimental procedures were conducted in strict accordance with the guidelines for the care and use of laboratory animals. The animal study protocol was approved by the Institutional Animal Care and Use Committee (IACUC) of Qinghai University (Approval No. SL-2023042, Approval Date: 2023.06.29).

Data Availability: The raw sequencing data (16S rRNA gene) have been deposited in the NCBI Sequence Read Archive (SRA), and the non-targeted metabolomics data have been submitted to the MetaboLights database. Accession numbers will be provided upon the formal acceptance of the manuscript. For further inquiries regarding the datasets, please contact the corresponding author.

Competing Interests: The authors declare there are no competing interests.

References

1. Liu X, Wei H, Shi H, Sha YZ, Wang JQ, Li SB, Lü WB, Guo XY, Pu XN, Luo YZ. Analysis of meat quality and fatty acid characteristics of grassland-grazing Tibetan sheep in different months [J]. Journal of Domestic Animal Ecology.
2. Li Q. Screening, Analysis and Functional Research of Disease-Resistant Immune Genes in Tibetan Sheep [D]. Qinghai University, 2020.
3. Johnson CL, Versalovic J. The human microbiome and its potential importance to pediatrics[J]. Pediatrics, 2012, 129(5): 950-960.
4. Mowat AM, Agace WW. Regional specialization within the intestinal immune system. Nat Rev Immunol. 2014 Oct;14(10):667-85.
5. ADOLPH TE, MAYR L, GRABHERR F, et al. Paneth cells and their antimicrobials in intestinal immunity[J]. CURR PHARM DESIGN, 2018, 24(10):1121-1129.
6. Gong Z, Ye G, Xu S, He X. The characteristics of intestinal flora of Tibetan sheep in different regions at high altitude were revealed based on metagenomic technique[J]. Heliyon, 2024, 10(14):e34380.
7. Zhao H, Mo Q, Kulyar M, Guan J, Zhang X, Luo X, Li J. Metagenomic analysis reveals a gut microbiota structure and function alteration between healthy and diarrheic juvenile yaks[J]. Animals, 2024, 14(8):
8. Li H, Zhang XA. Research Progress on the Mechanism and Application of Pueraria lobata in the Treatment of Inflammatory Bowel Disease [J]. Chinese Herbal Medicines, 2025, 56(04): 1428-1439.
9. Du Y, Gao Y, Hu M, Hou J, Yang L, Wang X, Du W, Liu J, Xu Q. Colonization and development of the gut microbiome in calves[J]. Journal of Animal Science and Biotechnology, 2023, 14: 46.
10. Yang X, Fan X, Jiang H, Zhang Q, Dui B, Zhang Q, Dang S, Long R, Huang X. Simulated seasonal diets alter yak rumen microbiota structure and metabolic function[J]. Frontiers in Microbiology, 2022, 13: 1006285.
11. Chen Y, Xiao L, Zhou M, Zhang H. The microbiota: a crucial mediator in gut homeostasis and colonization resistance[J]. Frontiers in Microbiology, 2024, 15: 1417864.
12. Yang DX. Prevention and Control of Peste des Petits Ruminants in Tibetan Sheep [J]. Animal Husbandry and Veterinary Science, 2020, 79(19): 139-140.
13. Xu BC, Li Z, Wang YZ, et al. Meta-Analysis of the Effects of Antimicrobial Peptides on Growth Performance, Diarrhea Rate and Immunoglobulin Levels in Piglets [J]. Chinese Journal of Animal Nutrition. 2020, 32(08):3584-3593.
14. Wang ZX, Huang YQ, Liu YH, et al. Inhibitory Mechanism of Antimicrobial Peptides from Paenibacillus aiyuanensis on Candida albicans Biofilm [J]. Food Science, 2024, 45(21):176-184.
15. Peng JJ, Chen YQ. Application of Insect-Derived Antimicrobial Peptides in Animal Husbandry Production [J]. Swine Industry Science, 2025, 42(02):87.
16. Yu W, Guo X, Li X, Wei Y, Lyu Y, Zhang L, Wang J, Shan A. Novel multidomain peptide self-assembly biomaterials based on bola structure and terminal anchoring: Nanotechnology meets antimicrobial therapy. Mater Today Bio. 2024 Aug 6;28:101183.
17. Ma X, Yang N, Mao R, Hao Y, Li Y, Guo Y, Teng D, Huang Y, Wang J. Self-assembly antimicrobial peptide for treatment of multidrug-resistant bacterial infection. J Nanobiotechnology. 2024 Oct 30;22(1):668.

 doi:10.20944/preprints202603.1006.v1

18. Zhang Z, Chen Y, Gao J, Yang M, Zhang D, Wang L, Zhang T, Cao Q, Mwangi J, He C, Li Y, Liu X, Jiang X, Kamau PM, Lai R. Orientational Nanoconjugation with Gold Endows Marked Antimicrobial Potential and Drugability of Ultrashort Dipeptides. Nano Lett. 2023 Dec 27;23(24):11874-11883.
19. Aphale D, Kulkarni A. Modifications and optimization of manual methods for polymerase chain reaction and 16S rRNA gene sequencing quality community DNA extraction from goat rumen digesta. Vet World. 2018 Jul;11(7):990-1000.
20. Mosley JD, Schock TB, Beecher CW, Dunn WB, Kuligowski J, Lewis MR, Theodoridis G, Ulmer Holland CZ, Vuckovic D, Wilson ID, Zanetti KA. Establishing a framework for best practices for quality assurance and quality control in untargeted metabolomics. Metabolomics. 2024 Feb 12;20(2):20.
21. Chiang JY. Bile acid metabolism and signaling. Compr Physiol. 2013 Jul;3(3):1191-1212.
22. Wang YN, Zhang ZH, Liu HJ, Guo ZY, Zou L, Zhang YM, Zhao YY. Integrative phosphatidylcholine metabolism through phospholipase A2 in rats with chronic kidney disease. Acta Pharmacol Sin. 2023 Feb;44(2):393-405.
23. He M, Qin CX, Wang X, Ding NZ. Plant Unsaturated Fatty Acids: Biosynthesis and Regulation. Front Plant Sci. 2020 Apr 23;11:390.
24. Law SH, Chan ML, Marathe GK, Parveen F, Chen CH, Ke LY. An Updated Review of Lysophosphatidylcholine Metabolism in Human Diseases. Int J Mol Sci. 2019 Mar 6;20(5):1149.
25. Qin, J., Li, R., Raes, J. et al. A human gut microbial gene catalogue established by metagenomic sequencing. Nature 464, 59–65 (2010).
26. Ren Q, Wang D, Han J, Liu Z, Wu Z. Lacrimispora sinapis sp. nov., isolated from pickled potherb mustard (Brassica juncea Coss.). Int J Syst Evol Microbiol. 2025 Feb;75(2):006675.
27. Xie G, Jiang R, Wang X, Liu P, Zhao A, Wu Y, Huang F, Liu Z, Rajani C, Zheng X, Qiu J, Zhang X, Zhao S, Bian H, Gao X, Sun B, Jia W. Conjugated secondary 12α-hydroxylated bile acids promote liver fibrogenesis. EBioMedicine. 2021 Apr;66:103290.
28. Jia W, Xie G, Jia W. Bile acid-microbiota crosstalk in gastrointestinal inflammation and carcinogenesis. Nat Rev Gastroenterol Hepatol. 2018 Feb;15(2):111-128.
29. Chong J, Zhou Y, Li Z, Li X, Zhang J, Cao H, Ma J, Ge L, Zhong H, Sun J. Hyodeoxycholic acid modulates gut microbiota and bile acid metabolism to enhance intestinal barrier function in piglets. Front Vet Sci. 2025 Jun 20;12:1610956.
30. Wang S, Zeng X, Yang Q, Qiao S. Antimicrobial Peptides as Potential Alternatives to Antibiotics in Food Animal Industry. Int J Mol Sci. 2016 May 3;17(5):603.
31. Xu Z, Wang T, Wang Y, Li Y, Sun Y, Qiu HJ. Short-chain fatty acids: key antiviral mediators of gut microbiota. Front Immunol. 2025 Jul 25;16:1614879.
32. Dias, B.d.C., Lamarca, A.P., Machado, D.T. et al. Metabolic pathways associated with Firmicutes prevalence in the gut of multiple livestock animals and humans. anim microbiome 7, 20 (2025).